# The hidden story in BaNiO 3 to BaNiO 2 transformation: adaptive structural series and NiO exsolution

Ángel M Arévalo-López, Marielle Huve, Pardis Simon, Olivier Mentré

Journal Name

COMMUNICATION

# The hidden story in $BaNiO_3$ to $BaNiO_2$ transformation: adaptive structural series and NiO exsolution.

Received 00th January 20xx,
Accepted 00th January 20xx

DOI: 10.1039/x0xx00000x

www.rsc.org/

Angel M. Arevalo-Lopez,[a] Marielle Huvé,[a] Pardis Simon,[a] and Olivier Mentré *[a]

**$BaNiO_3$ crystal to $BaNiO_2$ crystal transformation is reported. Contrary to an intuitive topochemical reduction, a two steps reaction was observed. In the first step, NiO exsolution occurs and intermediate $Ba_{1+x}NiO_3$ phases were obtained and isolated. A composite approach was used to solve the novel structure for x ~ 1/6 with charge ordered $Ni^{2+}$ and $Ni^{4+}$. We argue that this NiO exsolution is responsible for the increased oxygen enhanced reactivity recently reported. Upon re-oxidation, oxygen-defficient mixed valent $BaN^{i3/4+}O_{3-x}$ are obtained such that the full redox cycle is irreversible and goes through a diversity of structural and nickel valence adaptative oxides.**

The exsolution of metal during reduction of transition metal oxides is common in nickel based $ABO_3$ compounds, and was recently observed on the hexagonal perovskite polytype of $Ba_8Ta_6NiO_{24}$.[1] More rarely, structures based on oxo-anion frameworks can exsolve metal oxide upon oxidation. This results in complex depleted lattices after partial metal oxide removal, observed for instance in olivine-like $LiFe(PO_4)$, layered $BaFe_2(PO_4)_2$ and more recently in the Dumortierite $Fe_{13.5}(AsO_4)_8(OH)_6$ compounds,[2-4] the $Fe^{2+}/Fe^{3+}$ redox couple leaves Fe-deficient compounds with $\alpha$-$Fe_2O_3$ nano-particles decorating the surface. The possibility to exsolve other transition metal oxides seems appealing. However, a suitable crystal structure with the required metal redox capabilities (oxidation potential : $Ni^{2/3+} > Co^{2/3+} > Mn^{2/3+} > Fe^{2/3+}$) is difficult, it often results in stable trivalent iron ions ($Fe^{3+}$) but divalent $Ni^{2+}$, $Co^{2+}$ and $Mn^{2+}$ in oxides. To circumvent this stability, here we show an original path for NiO exsolution using moderate reduction of super-oxidized 2H-$BaNi^{4+}O_3$ into $BaNi^{2+}O_2$. The mechanism involves the appearance of nickel deficient 1D-$Ba_{1+x}NiO_3$ perovskites observed as reaction intermediates for the first time, the discovery of a new x ~1/6 member is reported.

$BaNiO_2$ can be directly prepared from a BaO/NiO mixture under inert atmosphere.[5] The alternative route via reduction of $BaNiO_3$ is rather controversial. It involves several reaction steps and versatile nickel oxidation states within structurally related 1D- crystal structures.[6-8] A number of intermediate phases have been proposed with various compositions that picture structural complexity rationalized only in the last decades. During the moderate $BaNiO_3$ reduction, several $BaNiO_{3-x}$ stoichiometries have been proposed,[9,10] culminating with a substoichiometric $BaNi_{0.86}O_{2.36}$ compound.[6] The later evidence and structural understanding in terms of composite structures of the $A_{1+x}NiO_3$ (A= Sr, Ni) series[11-14] helps to understand the $BaNi_{5/6}O_{5/2}$ oxide, first announced with supermixed valence +2,+3,+4 nickel.[13] This latter phase is considered as intermediate archetype during the structural transformation over the oxygen-evolution reaction (OER) redox cycling.[15] On the opposite, upon re-oxidation of $BaNiO_2$ the existence of a true oxygen deficient $BaNiO_{2.78}$ phase was verified.[16] In this same study, cycling the OER reaction gave the first clues of superficial NiO and NiOOH nanoparticles obtained from Ni exsolution. All of this gives an unclear panorama to be unraveled in here.

$BaNiO_3$ was prepared in molten KOH as previously reported.[17] It presents the ideal 2H hexagonal perovskite (*P6₃/mmc* with $a$ = 5.6386(1) Å and $c$ = 4.8092(3) Å), where $NiO_6$ octahedra share faces and form 1D infinite chains along the hexagonal $c$-axis. The X-ray diffraction (XRD) pattern confirms a single $Ni^{4+}$ phase, Fig. S1. Its reduction on heating in $N_2$ or Ar flow leads to similar results and was studied *in-situ* with high-temperature X-ray diffraction (HTXRD), differential thermal-analysis (DTA) and thermogravimetric analysis (TGA) (see Fig.1). X-ray photoelectron spectroscopy (XPS) was also studied.

The reduction occurs mainly in two steps. At *ca.* 500°C, $BaNiO_3$ transforms into trigonal $Ba_{1-x}NiO_3$ releasing nickel oxide by exsolution according to the reaction:

$(1+x)BaNiO_3 \rightarrow Ba_{1+x}(NiO_3) + x\,NiO + x\,O_2$ (1)

[a] *Univ. Lille, CNRS, Centrale Lille, ENSCL, Univ. Artois, UMR 8181 - UCCS - Unité de Catalyse et Chimie du Solide, F-59000 Lille, France.*
** olivier.mentre@ensc-lille.fr*

Electronic Supplementary Information (ESI) available: [details of any supplementary information available should be included here]. See DOI: 10.1039/x0xx00000x





Please do not adjust margins

The TGA smooth step denotes a progressive transformation through various x values. The structural features of $Ba_{1+x}NiO_3$ are complex but well understood crystallographically [18-22] as detailed below for the new x~1/6 case.

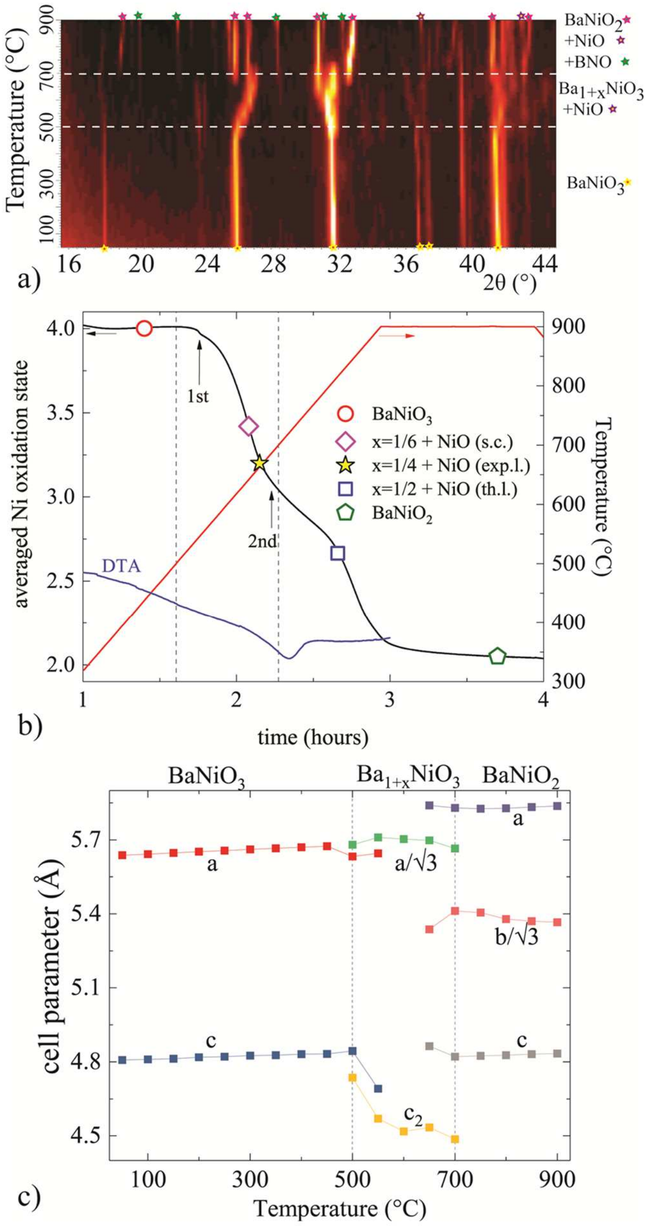


**Figure 1**: a) HT-XRD in flowing $N_2$ from $BaNiO_3$ to $BaNiO_2$ with label of the competing phases. b) TGA/DTA plots in same conditions along with marks for the observed intermediate $Ba_7Ni_6O_{18}$ (s.c. for single crystal data ; x = 1/6), the experimental limit $Ba_5Ni_4O_{15}$ (x = ¼) and the theoretical limit $Ba_3Ni_2O_6$ (x = ½). c) Reduced lattice parameters for the main identified phases (for the composite, $c_2$ refers to the [Ba] sublattice). Dashed lines are placed at 500 and 700 °C in the three plots.

Experimentally, $Ba_{1+x}NiO_3$ was observed up to x~1/4 at 700°C (exp.l. for experimental limit on fig.1b) where the TGA shows an inflexion with the appearing of $BaNiO_2$. It is far below the x = ½ theoretical limit (th. l. on Fig.1b) able to substain as discussed below. The reduction of $[BO_3]_\infty$ 1D-chains of face sharing octahedra ($B_O$) of the 2H-perovskite, induce the removal of $MO_3$ units which locally creates a trigonal prism ($B_P$) in the octahedral chains. This may be promoted by the poor ability to sustain oxygen deficiency in the ($AO_3$) hexagonal layers.[23,24]

The O/P sequence is versatile and it leads to a broad series of B deficient $A_{1+x}BO_3$ compounds, generally described as modulated composites between the $[A]_{1+x}$ and the $[BO_3]$ sublattices differing by their *c* cell parameters ($c_1$ vs $c_2$). Following the assumption that A, $B_O$ and $B_P$ are occupied by $Ba^{2+}$, $Ni^{4+}$ and $Ni^{2+}$ according to the $Ba_{1+x}Ni^{2+}{}_{P,x}Ni^{4+}{}_{O,1-x}O_3$ main formula, it is remarkable that an infinity of aliovalent charge ordered $Ni^{2+}$/$Ni^{4+}$ phases pave the way between $BaNi^{4+}O_3$ (x = 0) to the theoretical limit $Ba_{1.5}Ni^{2+}{}_{0.5}Ni^{4+}{}_{0.5}O_3$ (x = ½). This last phase corresponds to the $Ca_3Co_2O_6$-like with O-P sequence. Such structural evolution during reduction is highlighted by the gradual decrease of the $c_2$ cell parameter (between 500 and 700 °C in Figure 1c). The ratio of prismatic $Ni^{2+}$ gradually increases along with the amount of exsolved NiO. All of this occurs in the absence of a sharp DTA signal. XRD and DTA data suggest that this gradual reduction remains until ~650-700°C at x ~ ¼, *i.e.* much above the x = ½ limit. The similitude between the crystal structures involved during the process suggests topochemical reactions. In addition, the reduction of rod-like single crystals of $BaNiO_3$ preserves the shape and crystallinity of the starting products, which involve so-called single crystal to single crystal transformation by metal exsolution. However, some superficial damage is suffered due to this NiO exsolution, as seen by comparing pristine crystals (Figures 2a) and those after this first reduction step (650 °C, Figure 2b). This behaviour is similar to what was reported for $BaFe_{2-x}(PO_4)_2$ with decorating nanometric $Fe_2O_3$ islets.[25,26] As detailed below, the $Ba_{1+x}NiO_3$ phases are composite structures and the modulation between the two interacting sublattices, $\gamma=c_1/c_2$, is directly related to the crystal stoichiometry. We found $\gamma$ values between 0.55 and 0.58 after examination of the samples heated at 600, 650 and 700°C, see Fig.2c-e.

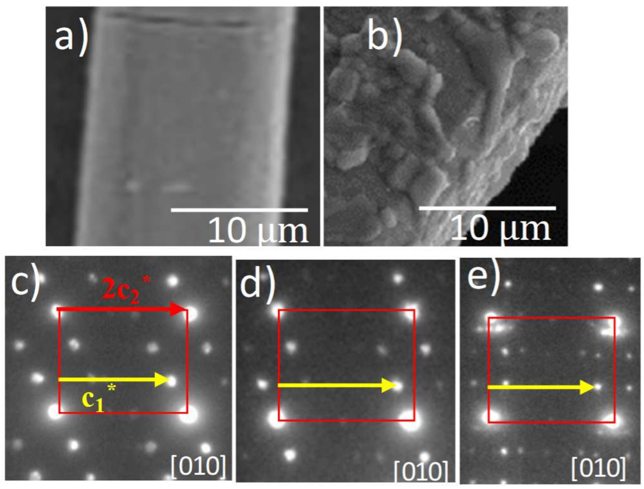


**Figure2**: a) as-prepared clean versus b) 650°C damaged crystal surface after the first reduction step. c-e) [010] ED patterns at 600, 650, 700°C showing the Ba sublattices with sizeable $c_2$* versus c1* ratio.

The second reaction step starts at ~700°C and corresponds to the appearing of the final $BaNiO_2$ and a second phase labelled

BNO. The DTA sharp peak shows a first order reaction. At 750 °C, the transformation of $Ba_{1+x}NiO_3$ into the $BaNiO_2$/BNO mixture is completed according to the reaction:

$Ba_{1+x}NiO_3 + xNiO \rightarrow (1-\rho)(1+x\ BaNiO_2) + \rho(BNO) + x\ NiO + O_2$ (2)

The XRD peaks assigned to BNO grow significantly until 900°C and subsist after cooling as long as the sample remains under flowing $N_2$. At this stage a significant amount of NiO remains (*i.e.* ~20w% of $BaNiO_2$), as refined using XRD data, see Figure S2. In air, BNO reacts with the exsolved NiO leading to a nearly single phase of $BaNiO_2$, see Figure S3. Therefore, BNO corresponds to an unstable $Ba_{1+x}Ni^{2+}O_{2+x}$ polytype, that is prompt to react with NiO to form $BaNiO_2$ under air. Therefore, the second reaction step is not topotactic anymore, at least for a significant part of the sample and $BaNiO_2$ appears nearly single phase only after air exposure. Concerning the mysterious BNO compound, its XRD pattern was indexed in an orthorhombic unit cell with $a$ = 5.4640(3) Å, $b$ = 8.8851(4) Å and $c$ = 7.1620(3) Å cell parameters. This compound is outside the scope of this article.

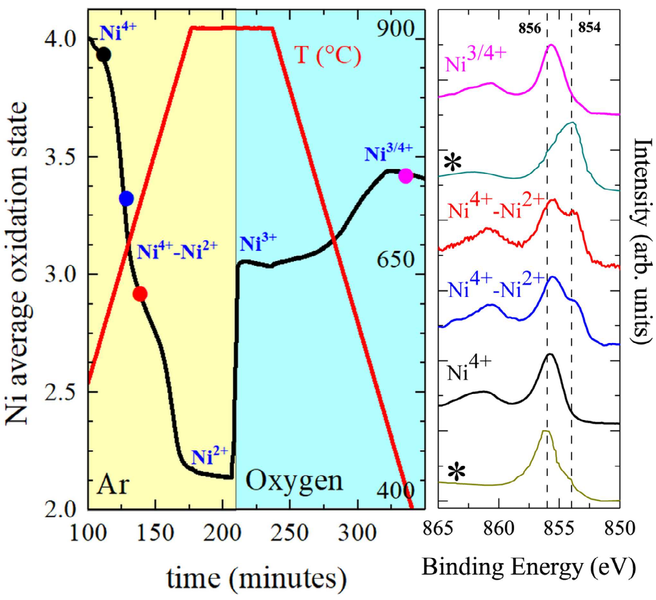


**Figure 3**: a) Full TGA history starting from $BaNiO_3$ with details of the charge segregation. b) XPS data for selected stages (color dots on a) of the reduction along with the reoxidation. Asterisk denotes data from ref. [27] for $BaNiO_3$ and $BaNiO_2$.

The second step collapses the structure and was verified by the observation of the crystal shapes. Increasing the temperature above 700°C clearly reveals shortening of the crystal sizes, typically by 2-3 times along the needle axis. According to (2), the transformation is reconstructive and the BNO should grow at the expense of $Ba_{1+x}NiO_3$ single domains. This reaction is not reversible and we have verified by TGA that the re-oxidation of $BaNiO_2$ in air is achieved until a single phase $BaNiO_{\sim 2.7}$ stoichiometry in agreement with the $BaNiO_{2.78}$ refined from powder neutron diffraction data.[15] Using single crystals, the full TGA cycle shown in Fig. 3, confirms an unusual redox path along with single crystal to single crystal topochemical transformations. After re-oxidation at 900°C, we identified a mixture of two mixed valent $Ni^{3/4+}$ 2H-$BaNiO_{3-x}$ types of crystals with distinct x values preliminary to full equilibrium into a single phase, see S4. XPS data also confirm these observations, Figure 3b shows the spectra for the initial $BaNiO_3$, two reduced phases and the reoxidized final stage, it also shows spectra for $BaNiO_3$ and $BaNiO_2$ from reference [27]. It can clearly be seen that the intermediate phases present both signals for $Ni^{4+}$ and $Ni^{2+}$, the limited exsolution of NiO as reduction product cannot explain the relative intensities between both maxima. The reoxidized compound is also much more similar to the $BaNiO_3$ spectra, in accordance with the TGA measurements.

Concerning the first reaction step, the continuous evolution of x in a wide range of composition enables the stabilization of discrete members. For instance, evidence of the reduction product $Ba_7Ni^{4+}{}_5Ni^{2+}{}_1O_{18}$, predicted to occur above 700 °C from the TGA (see Fig.1b) was given by single crystal XRD in the sample heated at 700°C and cooled down. The new isolated $Ba_{1.16}NiO_3$ structure presents a sequence of 5 octahedra per 1 trigonal prism (5O/1P) with an average nickel oxidation state of +3.666.

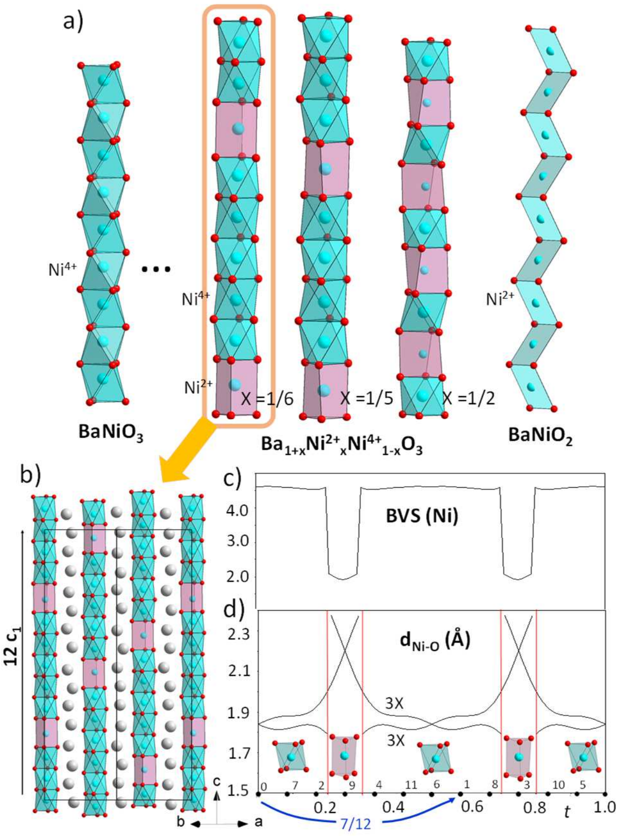


**Figure 4**: a) Structural sequence between $BaNiO_3$ and $BaNiO_2$ with b) 5O/1P approximant sequence in a commensurate a, b, 12 $c_1$ unit cell. b) Nickel bond valence sums along $t$, *i.e.* projection of x4 in the real space. c) evolution of the 6 Ni-O bond distances versus $t$. Number 0 to 11 allows the cell to cell iteration by translation of the modulation vector q = (0, 0, $\gamma$).

The crystal structure was refined in Jana2006 [28] as a composite structure, following the methodology first proposed by Evain et al.[20] The trigonal lattice parameters for the [NiO] and (1+x)[Ba] composite are refined to $a$ = 9.842(1) Å, $c_1$ = 2.5600(6) Å, $c_2$ = 4.4082(8) Å, leading to a modulation $\gamma = c_1/c_2$ = 0.58074 along the $c$ direction (*i.e.* 7/12 in a commensurate approximation). The super space group used is R-3m(00γ):P-3c1(00$\gamma^1$). The refinement validates the x ~ 1/6 value and 5O/1P sequence deduced from the relation $\gamma$ = (1+x)/2 available in these composite series. The final R values are 4.97%(all reflections), 3.84% (main), 12.83%(1st order satellites) and 12.71% (2nd order satellites) using positional waves of 4th, 1st, 4th orders and thermal parameters waves of 2nd, 1st and 0th orders for the three Ni, O and Ba atoms. The "ideal" transformation of the 1D-column during the reduction is shown on Fig.4a. The oxygen modulated occupancy is responsible for the octahedral *vs.* prismatic cavities and was modelled by a Crenel function.[22] The refinement in a commensurate approximation significantly increased the R% values, validating the incommensurate approach and implying that the 5O/1P sequence is sometimes broken. Fig.4c and 4*d* show the calculated Ni bond valence sum (BVS) and Ni-O distances projected in the real space along the *t* coordinate. On these figures, the cell counting from n to n+1 is performed by adding the q vector along *t* as idealized for a 12-unit cell sequence. In good agreement with the formula $Ba_{1+x}Ni^{2+}_xNi^{4+}_{1-x}O_3$ given above, the BVS clearly shows a complete $Ni^{2+}/Ni^{4+}$ charge ordering involved by the valence segregation in face-sharing O and P coordinations, which is valid in the full series of reduced phases in $BaNiO_{3-\delta}$. The same behaviour has been observed in the $Sr_{1+x}NiO_3$ series. It also confirms that $Ba_{1.2}NiO_3$ originally proposed with nickel +2, +3 and +4 supermixed valence[13] should only be in +2 and +4 oxidation states and probably requires an incommensurate-composite approach on the refinement of the data. Our XPS data also support this, however, sample reoxidation could occur and the presence of $Ni^{3+}$ cannot be ruled out a priori. Note that the cobalt case is different, taking into account $Co^{3+}$ low spin in the prisms of $Ca_3Co_2O_6$.[29]

On the other hand, recent claims of enhanced oxygen evolution reactions in this phases[15, 16] are questioned by the concomitant appearance of NiO in the reduction process known as a good electrocatalyst for water oxidation.[30]

In conclusion, NiO exsolution in reduced phases of $BaNiO_3$ was observed. In situ measurements show a two steps process with a gradual evolution from $BaNiO_3$ to $Ba_{1+x}NiO_3$ (1st step) and a more abrupt transformation to $BaNiO_2$ (2nd step) but keeping a single crystal to single crystal transformation for a part of the sample. The transformation goes through a diversity of structural and $Ni^{2+}/Ni^{4+}$ charge ordered intermediates. An original composite member was isolated and solved by single crystal diffraction with x ~ 1/6. The $Ni^{2+}/Ni^{4+}$ charge ordering obeys a 5 octahedra / 1 trigonal prims sequence. It also suggests the possibility of stabilization of tailor-made x values. In addition, this phenomenon is irreversible and the partial re-oxidation of the reaction product $BaNiO_2$ into $BaNi^{3+,4+}O_{3-x}$ increase the complexity in the redox properties of this fancy system. We argue that the observed NiO exsolution is responsible for the increased oxygen enhanced reactivity recently reported. The exsolution and then re-solution on NiO is very unusual that lead us to question whether other systems are quite as simple as we think. This will have implications in a wide range of catalytic systems, and also chemical fields such as 'oxygen storage' which use this exact type of chemistry to facilitate combustion and fuel cell operation.

There are no conflicts to declare.

## Notes and references

This work was carried out under the framework of the Marie Curie project KISS-ME, (Grant n° 750971) and LOVE-ME project supported by the ANR (Grant ANR-16-CE08-0023). The Fonds Européen de Développement Régional, CNRS, Région Nord Pas-de-Calais, and Ministère de l'Education Nationale de l'Enseignement Supérieur et de la Recherche are acknowledged for funding the X-ray diffractometers and microscopes. The authors thank L. Buryloa nd and F. Djelal for technical support.

[1] T. Pussacq, O. Mentré, F. Tessier, A. Lofberg, M. Huvé, J. Guerrero Caballero, S. Colis and H. Kabbour, *J. Alloys Compd.*, 2018, **766**, 987.
[2] S. Hamelet, M. Casas-Cabanas, L. Dupont, C. Davoisne, J.M. Tarascon and C. Masquelier, *Chem. Mater.*, 2011, **23**, 32.
[3] R. David, H. Kabbour, D. Filimonov, M. Huvé, A. Pautrat, O. Mentré, *Angew. Chem. Int. Ed.*, 2014, **53**, 13365.
[4] O. Mentré, I. Blazquez-Alcover, S. Garcia-Martin, M. Duttine, A. Wattiaux, P. Simon, M. Huvé, S. Daviero-Minaud,
Inorg. Chem, 2018, in press.
[5] R. Gottschall and R. Schöllhorn, *Solid State Ion.,* 1993, **59**, 93.
[6] R. Gottschall, R. Schöllhorn, M. Muhler, N. Jansen, D. Walcher, P. Gütlich, *Inorg. Chem*., 1998, **37**, 1513.
[8] J. A. Campá, E. Gutiérrez-Puebla, M.A. Monge, I. Rasines anc C. Ruíz-Valero, *J. Solid State Chem.,* 1994, **108**, 230.
[9] J. DiCarlo, I. Yazdi, A. J. Jacobson, A. Navrotsky, *J. Solid State Chem.*, 1994, **109**, 223.
[10] H. Shibahara, *J. Solid State Chem.*, 1987, **69**, 81.
[11] R. Gottschall and R. Schollhorn, *Inorg. Chem.*, 1998, **37**, 1513.
[12] F. Abraham, S. Minaud and C. Renard, *J. Mater. Chem.*, 1994, **4**, 1763.
[13] J. Campa, E. Gutierrez-Puebla, A. Monge, I. Rasines and C. Ruiz-Valero, *J. Solid State Chem.*, 1996, **126**, 27.
[14] M. Huvé, C. Renard, F. Abraham, G. Van Tendeloo and S. Amelinckx, *J. Solid State Chem.,* 1998, **135**, 1.
[15] J.G. Lee, J. Hwand, H. J. Hwang, O. S. Jeon, J. Jand, O. Kwon, Y Lee, B. Han and Y-G. Shul, *J. Am. Chem. Soc.,* 2016, **138**, 3541.
[16] M. Retuerto, F. Calle-Vallejo, L. Pascual, P. Ferrer, A. García, J. Torrero, D. Gianolio, J. L. G. Fierro, M. A. Pena, J. A. Alonso and S. Rojas, *J. Power Sources,* 2018, **404**, 56.
[17] J. DiCarlo, I. Yazdi, A. J. Jacobson, A. Navrotsky, *J. Solid State Chem.*, 1994, **109**, 223
[18] A. El Abed, S. E. Elqebbaj, M. Zakhour, M. Champeaux, J.M. Perez-Mato, J. Darriet, *J. Solid State Chem.,* 2001, **161**, 300.
[19] M. Zakhour-Nakhl, F. Weill, J. Darriet, J.M. Perez-Mato, *Int. J. Inorg. Chem*., 2000, **2**, 71.
[20] M. Evain, F. Boucher, O. Gourdon, V. Petricek, M. Dusek, and P. Bezdicka, *Chem. Mater.*, 1998, **10**, 3068.
[21] O. Gourdon, V. Petricek, M. Dusek, P. Bezdicka, S. Durovic, D. Gyepesova, M. Evain, *Acta cryst*., 1999, **B55**, 841.
[22] P. Roussel, O. Perez, E. Quarez, H. Leligny, O. Mentré, *Z. Kristallogr.*, 2010, **225**, 1.
[23] J. J. Adkin and M. A. Hayward, *Chem. Mater.*, 2007, **19**, 755.
[24] O. Mentré, M. Iorgulescu, M. Huvé, H. Kabbour, N. Renaut, S. Daviero-Minaud, S. Colis, P. Roussel, Dalton Trans., 2015, **44**, 10728.
[25] I. Blazquez Alcover, S. Daviero-Minaud, R. David, D. Filimonov, M. Huvé, J.P. Attfield, H. Kabbour, O. Mentré, *Inorg. Chem*., 2015, **54** , 8733.
[26] I. Blazquez Alcover, R. David, S. Daviero-Minaud, D. Filimonov, M. Huvé, P. Roussel, H. Kabbour, O. Mentré, Cryst. Growth Design, 2015, 15, 4237.
[27] R. Gottschall, R. Schollhorn, M. Muller, J. Jansen, D. Walcher, P. Gutlich, Inorg. Chem. 1998, **37**, 1513.
[28] V. Petricek, V. Eigner, M. Dusek and A. Cejchan, *Z. Kristallogr. Cryst. Mater.,* 2016, **231**, 583.
[29] A. Maignan, V. Hardy, S. Hébert, M. Drillon, M. R. Lees, O. Petrenko, D. Mc K. Paul, D. Khomskii, J. Mater. Chem. 2004, **14**, 1231.
[30] C. C. L. McCrory, S. Jung, J. C. Peters and T. F. Jaramillo, J. Am. Chem. Soc., 2013, **135**, 16977.